

Lifted Temperature Minimum During the Atmospheric Evening Transition

E. Blay–Carreras¹, E. R. Pardyjak², D. Pino^{1,3}, S. W. Hoch⁴, J. Cuxart⁵, D. Martínez⁶, and J. Reuder⁷

¹Department of Applied Physics, Universitat Politècnica de Catalunya-BarcelonaTech, Barcelona, Spain.

²Department of Mechanical Engineering, University of Utah, Salt Lake City (UT), USA.

³Institute for Space Studies of Catalonia (IEEC–UPC), Barcelona, Spain.

⁴Department of Atmospheric Sciences, University of Utah, Salt Lake City (UT), USA.

⁵Grup de Meteorologia, Departament de Física, Universitat de les Illes Balears, Palma de Mallorca, Spain.

⁶Center for Applied Geoscience, University of Tübingen, Tübingen, Germany.

⁷Geophysical Institute, University of Bergen, Bergen, Norway.

Correspondence to: E. Blay–Carreras (estel.blay@upc.edu)

Abstract. Observations of Lifted Temperature Minimum (LTM) profiles in the nocturnal boundary layer were first reported in 1932. It was defined by the existence of a temperature minimum some centimeters above the ground. During the following decades, several research studies analyzed this phenomenon verifying its existence and postulating different hypothesis about its origin.

The aim of this work is to study the existence and characteristics of LTM during the evening transition by using observations obtained during the Boundary Layer Late Afternoon and Sunset Turbulence (BLLAST) campaign. Data obtained from two masts instrumented with thermocouples and wind sensors at different heights close to the ground, and a mast with radiometers are used to study the role of mechanical turbulence and radiation in LTM development.

The study shows that LTM measurements can be detected under calm conditions during the day–night transition, several hours earlier than reported in previous work. These conditions are fulfilled under weak synoptic forcing during local flow shifts associated with a mountain–plain circulation in relatively complex orography. Under these special conditions, turbulence becomes a crucial parameter in determining the ideal conditions for observing LTM measurements. Additionally, LTM observed profiles are also related to a change in the atmospheric radiative characteristics under calm conditions.

1 Introduction

A Lifted Temperature Minimum (LTM) profile is characterized by an elevated temperature minimum close to the surface. Depending on the ground characteristics it is typically located between 10 and 50 cm above the surface and observed at night. After sunset, if cloudless and calm conditions exist and ground and air emissivities have similar values, the layer just above the ground can cool radiatively faster than the ground itself and a minimum temperature appears several centimeters above the surface. LTM measurements have been studied by means of observations (Ramdas and Atmanathan, 1932; Lake, 1956; Raschke and Atmanathan, 1957; Oke, 1970), numerical simulations (Zdunkowski, 1966; Vasudeva Murthy et al., 1993; Narasimha and Vasudeva Murthy, 1995; Vasudeva Murthy et al., 2005) and laboratory experiments (Mukund et al., 2010, 2014).

Ramdas and Atmanathan (1932) provided for the first time a detailed description of the unexpected temperature minimum neglecting advective effects and suggested that the LTM might be related with radiation from the ground and the lower layer of the atmosphere. Several years later, Lake (1956), and Raschke and Atmanathan (1957) confirmed the results obtained by Ramdas and Atmanathan (1932), discarding instrumental errors by using more complex instruments. Raschke and Atmanathan (1957) took measurements over different terrain types to verify that LTM measurements are not produced by advection and defined three different types of temperature profiles, distinguishing between profiles with the minimum temperature at the ground, LTM measurements

and profiles caused by advection. Additionally, they made measurements at different latitudes to prove that the phenomenon was not restricted to the tropics. On the contrary, Geiger (1965) showed some skepticism about the existence of LTM measurements. For instance, he wondered why LTM measurements are not overturned by convective instability. He was also concerned about the precision of the measurements close to the ground. Later on, Zdunkowski (1966) suggested the existence of a haze layer near the ground to explain the appearance of the LTM. Nevertheless, this approach was discarded because this layer was never observed and the thermal diffusivity required for its explanation was not realistic (Narasimha, 1994).

More recent studies have shown that LTM measurements are common over different natural, e.g. bare soil, snow and short grass (Oke, 1970) and artificial surfaces such as concrete or thermofoam (Mukund et al., 2010, 2014). Mukund et al. (2014) studied in detail the importance of surface characteristics for the appearance of LTM measurements. They demonstrated, by studying LTM formation over different surfaces (aluminum, thermofoam and concrete), that decreasing surface emissivity increases the intensity of a LTM and the near-ground temperature gradient. Lowering surface emissivity with respect to the overlying atmosphere can act to change the temperature profile from a minimum temperature occurring at the ground to an elevated temperature minimum. Therefore, terrain with an emissivity close to that of the overlying air favors LTM formation. Narasimha (1991, 1994) summarized the main mechanisms related to the occurrence of LTM measurements. In his first summary, he introduced a brief description of a model, which was later described in detail in Vasudeva Murthy et al. (1993). They hypothesized that radiative cooling depends on ground emissivity and the air emissivity gradient. When the air emissivity gradient is large, the temperature of the air close to the ground decreases faster than the temperature of the ground and a LTM can be observed. Even though the model presented a detailed solution for the air temperature evolution considering surface emissivity, ground cooling and turbulence, it did not include a detailed discussion of the energy budget near the ground, which was introduced afterwards by Narasimha and Vasudeva Murthy (1995).

Apart from ground thermal characteristics, calm conditions with low mechanical turbulence are crucial to observe a LTM. For instance, LTM intensity is weaker for high roughness length surfaces because it increases both turbulence and emissivity (Oke, 1970). Moreover, field measurements (Ramdas and Atmanathan, 1932; Lake, 1956; Raschke and Atmanathan, 1957; Oke, 1970) and models (Vasudeva Murthy et al., 1993; Narasimha and Vasudeva Murthy, 1995; Vasudeva Murthy et al., 2005) show that advection was weak when a LTM was observed. LTM has only been reported for a small number of cases where the friction velocities was above 0.1 ms^{-1} , and in those cases it was destroyed relatively quickly (Vasudeva Murthy et al., 2005).

Vasudeva Murthy et al. (1993) were the first ones to suggest a model which appears to be in good agreement with observations. They studied the importance of radiative, conductive and convective fluxes during LTM events. This model was accepted until Mukund et al. (2010) and Ponnulakshmi et al. (2012) identified an error in the calculations of Vasudeva Murthy et al. (1993) and introduced a new model based on the work by Edwards (2009a). This model includes the importance of suspended solid or liquid particles, which can act as a cooling mechanism. Narasimha (1991); Vasudeva Murthy et al. (2005); Mukund et al. (2010, 2014) pointed out the importance of radiation in the formation of LTM measurements. Mukund et al. (2010) confirmed that near the surface, radiative cooling can be orders of magnitude greater than values elsewhere in the boundary layer. With very light winds, the role played by turbulence is nearly negligible compared with the radiation. Therefore, temperature evolution is mainly governed by the radiation timescale (Vasudeva Murthy et al., 2005). Moreover, Mukund et al. (2014) showed that a heterogenous distribution of the aerosol concentration can cause a hyper-cooling close to the surface, which modifies the atmospheric radiative cooling.

Other hypothesis to explain the appearance of LTM measurements (or the temperature maximum at upper levels, around 20–30 cm) during the night, in stable conditions is based on the competition between the radiative warming of the lower layers (up to 50–70 cm) of the atmosphere over a rapidly cooling surface and the turbulence cooling (Savijarvi, 2006, 2014; Edwards, 2009a,b). The first process would drive the heat budget at 20–30 cm, but turbulence cooling would temporarily be dominant around 10–15 cm.

Daytime LTM measurements have been reported when near-surface temperature inversions occur under specific conditions over the open Arabian Sea during the summer monsoon season (Bhat, 2006). These atmospheric conditions, characterized by strong surface winds and high levels of sea salt particle concentration in the boundary layer, are far away from the conditions presented at night or here.

In summary, LTM measurements vary depending on surface characteristics (emissivity and thermal inertia), prevailing wind conditions (turbulence) and atmospheric radiation. In contrast with previous studies, we analyze LTM occurrences during the evening transition period. It is during this period when the largest radiative cooling occurs (Sun et al., 2003). Our research objectives are to study the relevance of wind characteristics driven by orography, turbulence, characterized by the Richardson number and the deviation of the instantaneous wind speed from the mean and radiation on the appearance of LTM during the evening transition.

The study of the appearance of LTM measurements, besides increasing the knowledge of the physics of the surface layer, it can be also relevant for agriculture. Lifted temperature minimum can modify the occurrence of frost, which has adverse effect on crops (Lake, 1956). Moreover, it can help to describe the presence of radiation fog, as it is shown in the

article, the presence of LTM is related with a variation of the radiation (Mukund et al., 2014).

The paper is structured as follows. In Sect. 2, we explain the measurements used in this study, taken during the Boundary Layer Late Afternoon and Sunset Turbulence (BLLAST) campaign. In Sect. 3, the temperature profiles are analyzed in detail and LTM characteristics are described. Section 4 investigates and presents the variables influencing LTM: wind characteristics and friction velocity, turbulence and radiation. Finally, Sect. 5 summarizes the results.

2 Measurements

To investigate LTM measurements during the evening transition, we analyze measurements acquired during the BLLAST field experiment (Lothon et al., 2014). This campaign was performed from 14 June to 8 July 2011 in southern France, near to the Pyrenees Mountains. The campaign site extended over an area of approximately 100 km² covered with heterogeneous vegetation, mainly grass, corn, moor and forest.

The most salient BLLAST objective was to obtain a detailed set of meteorological observations during the evening transition to better understand the physical processes that control it. For example, improved understanding of the effects of entrainment across the boundary layer top, surface heterogeneity, horizontal advection, clouds, radiation and gravity waves on the evening transition.

During intensive observational periods (IOPs), the atmosphere was heavily probed by in situ measurements from masts, towers, tethered balloons, radiosondes and manned and unmanned airplanes, as well as remote sensing instruments such as LIDAR and RADAR wind profilers.

For the present work, the near surface temperature evolution is analyzed using the measurements taken at two masts (T1 and T2) separated by approximately 468 m. Figure 1 shows a plan view of T2 area and a side view of the T1 and T2 instruments. T1 was located at 43.1275° N–0.36583° E and T2 at 43.1238° N–0.36416° E. T1 was a 10-m mast instrumented with four Campbell Scientific CSAT3 Sonic Anemometer Thermometers and Campbell Scientific E-TYPE model FW05 (12.7 μm diameter) Fine Wire (FW) thermocouples at 2.23, 3.23, 5.2 and 8.2 m. Closer to the ground, there were four additional FW05 12.7 μm FWs at 0.091, 0.131, 0.191 and 0.569 m which were only installed during the IOPs. Temperature data at T1 were recorded at 20 Hz. The influence of direct or indirect solar radiation has been taken into account in the measurements. Moreover, Campbell (1969) showed, as the size of the thermocouple goes down, the radiative influence is reduced. For a 25 μm sensor a 0.1 K of error was observed. Our sensor is half that size hence the error of the instrument should be lower than 0.1 K, which is smaller than the values of the LTM intensity.

T2 was a 2-m mast with eight FW3 (76.2 μm diameter) FWs located at 0.015, 0.045, 0.075, 0.14, 0.3, 0.515, 1.045

and 1.92 m recording temperature data at 10 Hz. Additionally, separated approximately 2 m from T2, there was also a Campbell Scientific CSAT3 at 1.95 m, recording data at 20 Hz. To unify the measurements taken by the different instruments, all the recorded data were averaged over 5 min intervals (De Coster and Pietersen, 2011). This information was complemented with an estimation of the skin temperature provided by a Campbell Scientific IR120 infrared remote temperature sensor pointing towards surface. This infrared sensor measured temperature with a sampling frequency of 3 Hz before 21 June 2011 and of 1 Hz after this day.

Near T2, one Kipp & Zonen CNR1 net radiometer was installed. The CNR1 sensor is able to measure upwelling and downwelling components of both the shortwave solar (0.305–2.8 μm) and terrestrial radiation (5–50 μm) separately. The CNR1 was installed at 0.8 m above the ground.

The ground characteristics below both masts were conducive to observe LTM measurements (Mukund et al., 2014). The ground in both cases was covered by long grass, which has an emissivity of 0.986 (Gayevsky, 1952). The vegetation cover has low thermal conductivities which varies from 0.05 to 0.46 W m⁻¹ K⁻¹ (Campbell, 1998). However, the surface surrounding T1 was covered by long grass, while the T2 surface had some cut grass over the terrain, which could cause some heterogeneity in the surface thermal properties.

Oke (1970) pointed out that, over grass-covered surfaces, the minimum temperature during the night can be found just above the grass instead of right at the surface. This phenomenon, which is associated with the vegetative canopy, is sometimes confused with a LTM. Oke (1970) observed a LTM at 0.02 m above the grass. In our case study, the grass height is short, around 0.03–0.07 m, and the observed LTM height occurred above 0.1 m from the ground, that is always above the grass.

For the following analysis, we selected different favorable IOPs with good data availability from the T1 and T2 areas. The analysis is based on the observations taken on 24, 25, 27, 30 June and 1 and 2 July 2011. During these IOPs, we have measurements from both towers, the infrared surface temperature sensor and the radiometer. These IOPs were clear and calm days with a mountain–plain circulation characterized by weak northerly winds during the day switching to southerly at night. The synoptic situation did not show any notable perturbation.

3 Observed LTM characteristics

During the BLLAST campaign, when LTM occurred, it was observed in both masts. Figure 2 shows the evolution of potential temperature profiles where a LTM is observed on 24 June 2011 (top panels) and 1 July 2011 (bottom panels) recorded at T1 (left) and T2 (right). The LTM can be observed on both days at both masts.

As illustrated in Fig. 3, three sensors on each tower were used to detect and characterize LTM measurements. First, the location of the minimum temperature was identified (θ_{base}).³²⁵ Next, the sensor closest to the ground was defined as LTM \blacktriangledown . Finally, the sensor located just above the base sensor (LTM \blacktriangle)²⁷⁵ was identified. a LTM is observed if:

$$\theta_{base} - \theta_{LTM\blacktriangledown} < 0 \quad \text{and} \quad \theta_{LTM\blacktriangle} - \theta_{base} > 0. \quad (1)$$

During this period, LTM intensity is calculated following (Mukund et al., 2010):

$$LTM_{intensity} = \theta_{base} - \theta_{LTM\blacktriangledown}. \quad (2)$$

The LTM duration was defined as the period when the LTM conditions outlined above were fulfilled. Table 1³³⁵ presents a summary of the following LTM characteristics for the different IOPs: height, intensity absolute values) and duration of the phenomenon.²⁸⁵

A LTM was observed during the evening transition for all IOP days except on 27 June 2011. A LTM forms at similar heights on both towers. For example, at T1 a height of³⁴⁰ around 0.131 m was typical, while LTM heights were between 0.075 m and 0.14 m (except on 25 June 2011) at T2. Unfortunately, limitations in the vertical resolution of the measurements prevent a more precise determination of the LTM heights. In spite of this consistency, there are clear differences³⁴⁵ between the detailed LTM characteristics on different IOPs and at the different towers. On 24 June 2011, a LTM was observed during a 10 min period at T1 and for 40 min at T2. Greater LTM-intensity (0.7 K) was observed at T2 compared to T1 (0.35 K). On 25 June 2011, a LTM was detected³⁵⁰ at T2 at a slightly higher level, around 0.3 m with an intensity of 0.5 K. This height is in the range of LTM-heights reported by Raschke and Atmanathan (1957). On 25 June 2011, FWs were installed at T1 after 19:30 UTC, therefore, LTM comparisons cannot be made.³⁵⁵

A completely different situation was observed on 27 June 2011; with no clear LTM development. T2-measurements showed indications of a LTM formation which did not progress.

On 30 June 2011, T1 showed a slightly lower-intensity³⁶⁰ (0.3 K) LTM starting around 18:00 UTC and lasting less than 20 min. A slightly lower-intensity LTM was also observed at T2 with an intensity of 0.5 K. On 1 July 2011 a clearly marked (0.7 K) LTM was observed at T2 for a duration of one hour. On the other hand, T1 showed a less pronounced LTM³⁶⁵ (0.35 K), which persisted only 20 min. Finally, on 2 July 2011 T2 showed a LTM intensity of around 0.5 K with a duration of more than one hour. However, T1 showed an intensity (0.35 K) with a duration of 40 min.

Due to the variations in sensor heights at the two loca-³⁷⁰ tions, the LTM intensity can vary from one tower to the other one. Day to day variations at a single location, however, can be compared. Specifically, our definition of LTM intensity

is based on the temperature measured closest to the ground, that, in order to detect a LTM needs to be warmer than the LTM. The elevation of the sensor closest to the ground differs for our two observations at T1 and T2 (about 9 and 1.5 cm, respectively), thus the two locations' intensities are not strictly comparable. As shown in Table 1, the LTM intensity at T2 is always roughly twice the value observed at T1, which is most likely due to the fact that the lowest thermocouple at T1 is still influenced by the cold air associated with the LTM and an additional increase in temperature towards the surface is not resolved.

4 Variables influencing LTM development

4.1 Mean wind characteristics

The analysis of wind conditions is crucial for understanding the influence of mechanical turbulence on the formation of LTM measurements. Since all of the IOPs presented in the analysis were associated with weak synoptic forcing, orography will be the main driver of surface winds during the evening transition (Nadeau et al., 2013).

Figure 4 shows the temporal evolution of the averaged 2-m wind speed and direction every 5 min observed at T1 and T2. The observed wind directions shown in Figs. 4a, b clearly indicate for most of the days a typical mountain-plain circulation (Whiteman, 2000): daytime plain-mountain wind (northerly over the Lannemezan Plateau toward the Pyrenees), early evening calm conditions and nighttime mountain-plain wind (southerly). The wind speed observations (see Figs. 4c, d) indicate slightly weaker winds at T2, most likely due to the presence of trees nearby T2 and by the differences in the surface cover. Before 17:30 UTC, 2.5 and 2 ms⁻¹ wind speeds were observed at T1 and T2 respectively. At 17:30 UTC, the wind speed started to decrease except on 27 June 2011, indicating the beginning of the evening calm period. However, the decrease rate was not the same for all the IOPs, being faster on 24 June, 1 and 2 July 2011. The wind speed continued to decrease until 18:30–19:00 UTC when the wind was around 0.5 ms⁻¹ at both masts. During this period, the wind direction turned from northerly to southerly progressively (see Figs. 4a, b). After 19:00 UTC, surface flows from the mountains dominated, with increasing wind speed (see Figs. 4c, d).

In order to analyze why the wind-speed decay during the evening was different for the analyzed days, a WRF-mesoscale simulation (Skamarock, 2008) was performed with 3 km horizontal resolution from 29 June at 00 UTC until 3 July 2011 at 00 UTC. When analyzing the atmospheric conditions at low levels during the evening, a surface northerly wind is simulated at Lannemezan (43° 12' N–0.39° E) during the three days. However, on 30 June 2011 this northerly wind is simulated until a later hour than on 1 and 2 July 2011. This is due to the lower temperatures sim-

ulated at the Pyrenees mountain range on 30 June 2011 (not shown). A similar reason could explain the lowest wind decrease observed on 25 June 2011.

In stable conditions, Oke (1970) postulated that the wind speed at 0.25 m must be less than 0.4 m s^{-1} to observe a LTM over short grass. In our study case, sensors measuring wind speed were at 2 m. Therefore, we need to extrapolate this value to 0.25 m to be able to compare with previous results. To do this a log-law approximation for neutral stability conditions was utilized, namely:

$$v \approx v_{\text{ref}} \frac{\ln(z/z_0)}{\ln(z_{\text{ref}}/z_0)}, \quad (3)$$

where v is the wind speed at height z , v_{ref} is the wind speed at height $z_{\text{ref}} = 2 \text{ m}$, and z_0 is the roughness length (0.03 m in our case). The results from this approximation show that for all the analyzed days except on 27 June 2011, the wind speed at 0.25 m is below 0.4 m s^{-1} .

4.2 Turbulence

The gradient Richardson number (Ri_g) is a crucial parameter in the study of the LTM during stable night conditions. Oke (1970) observed that $Ri_g > 0.1$ is needed to observe a LTM over different terrain in stable conditions. The gradient Richardson number is defined as (Stull, 1988):

$$Ri_g = \frac{g}{\theta_v} \frac{\overline{\partial\theta_v/\partial z}}{(\overline{\partial U/\partial z})^2 + (\overline{\partial V/\partial z})^2}, \quad (4)$$

where g is the gravity acceleration, θ_v is the virtual potential temperature, and U , V the horizontal wind components.

To estimate Ri_g , potential temperature vertical gradient was computed using the $\theta_{\text{LTM}\blacktriangle}$ and θ_{base} , as by definition, it is not possible to observe a LTM unless the $\overline{\partial\theta_v/\partial z}$ is positive directly above θ_{base} the height where the LTM is observed. Moreover, as we do not have measurements of the wind speed neither at LTM height or at $\text{LTM}\blacktriangle$, we approximate the U and V using Eq. 3. Figure 5 shows the temporal evolution of Ri_g during the evening transition obtained by using the data measured at T1 on all the studied days. As expected, as the stable surface layer develops, Ri_g significantly increased for all the days studied, except 27 June 2011, when Ri_g remains nearly constant and close to zero. During this day, a LTM was not observed because large mechanical turbulence in the lower part of the boundary layer existed.

An opposite situation occurred on 24 June and 1 and 2 July 2011. On these days a large increase of the Ri_g values is observed when Ri_g become positive and LTM appeared. The large increase of the Ri_g values is related to a fast decrease of mechanical turbulence. Therefore, on these three days LTM measurements were clearly observed with a large LTM intensity. 25 and 30 June 2011 have a less pronounced increase of the Ri_g values. These days have a smoother decrease of turbulence as well as a lower intensity of LTM.

As mentioned, Oke (1970) suggested a minimum Ri_g threshold for LTM formation of $Ri_g \gtrsim 0.1$. During nighttime, when the main destabilizing force is mechanical turbulence, Ri_g can be used to define the conditions for observing LTM measurements. However, this Ri_g threshold cannot be compared with our results because we observe a LTM when $\overline{\partial\theta_v/\partial z}$ is changing at the surface. Therefore, we cannot define an exact threshold for LTM formation and we focus our analysis in the change of the increase rate of the Ri_g values.

Decrease of mechanical turbulence during the afternoon transition can be also studied by using friction velocity (u_*). Figure 6 shows the temporal evolution of u_* at 2 m during the evening transition for all the studied days with a 5 min average. Due to the orography, during the afternoon, u_* decreased from around 0.25 m s^{-1} to values below 0.1 m s^{-1} (around 18:30 UTC at T1 and 18:00 UTC at T2). Afterwards it slightly increases but remains at lower values. Vasudeva Murthy et al. (2005) pointed out that a LTM can occur with friction velocities greater than about 0.1 m s^{-1} , but the layer slowly fades away. In our study case, during most of the IOPs u_* was reduced to values lower than 0.1 m s^{-1} shortly after the LTM occurrence, except on 27 June 2011, when friction velocity clearly presented values higher than 0.1 m s^{-1} during the evening transition at both masts. Therefore, during this day turbulence prevented the appearance of a LTM. Moreover, on 30 June 2011 u_* had low values but only during a short period during which a LTM occurred (see Figs. 6a, b).

Mukund et al. (2010) used wind speed fluctuations to analyze turbulence and its influence on LTM occurrence. Figure 7 shows the horizontal wind speed measured at 20 Hz and its mean value (a 500 s moving average) for two different IOPs, 24 June and 27 June 2011, which represent the most extreme cases. The LTM occurrence on 24 June (see Table 1) is associated with a clear decrease not only of mean wind speed but also of wind speed fluctuations (see Fig 7a). On the contrary, on 27 June, when a LTM is not observed, Fig. 7b shows that neither mean wind speed nor turbulence intensity decrease during the evening transition. By comparing these facts with the parameters described in Table 1, we can directly relate turbulence and mean wind velocity with the intensity of the LTM. IOPs with a clear decrease on turbulence during afternoon transition, such as 24 June, 1 July or 2 July 2011, present larger LTM-intensity. Those days with a lower or non-existing decrease of wind speed fluctuations have a less pronounced LTM or a LTM is not present.

4.3 Radiation

Narasimha (1991); Vasudeva Murthy et al. (2005) and Mukund et al. (2010, 2014) pointed out the radiative origin of LTM. For this reason, we also analyze the radiation measurements taken by the radiometers located near T2. Unfortunately, during all the days of the campaign a shadow produced by the 60-m tower located 160 m to the north-

west of T2 affected the shortwave and net radiation measurements. Consequently, here we can only analyze the upwelling longwave radiation recorded by the Kipp & Zonen CNR1 radiometer located at 0.8 m. Additionally, we estimate longwave radiation at the LTM height by using the conservation of heat equation (Stull, 1988):

$$\frac{\partial \bar{\theta}}{\partial t} + \bar{U}_j \frac{\partial \bar{\theta}}{\partial x_j} = \nu_\theta \frac{\partial^2 \bar{\theta}}{\partial x_j^2} - \frac{1}{\bar{\rho} C_p} \frac{\partial Q^*}{\partial x_j} - \frac{L_v E}{\bar{\rho} C_p} - \frac{\partial(\overline{u'_j \theta'})}{\partial x_j}, \quad (5)$$

where x_j represents (x, y, z) for $j = (1, 2, 3)$, ν_θ is the kinematic molecular diffusivity for heat in air, Q^* is the net radiation, L_v is the latent heat of vaporization of water, E is the phase change rate, ρ is density of the air, C_p is the specific heat at constant pressure for moist air and u_j is the wind components (u, v, w) for $j = (1, 2, 3)$.

The first term represents the tendency of the temperature, the second term describes the advection of heat by the mean wind. The third term is the mean molecular conduction of heat, the next term represents the net radiation flux divergence, the fifth term describes the latent heat release and the last term is the divergence of the turbulent heat flux. Despite large values of latent heat were measured at noon during BLLAST campaign, the fifth term of conservation of heat equation, is smaller in comparison with the other terms. This term on 1 July 2011, for instance, was approximately 0.15 K m s^{-1} during daytime, but decreased to values close to 0.01 K m s^{-1} .

If we consider very light winds, horizontal homogeneity and neglect subsidence, the heat equation can be written as:

$$\frac{\partial \bar{\theta}}{\partial t} = \nu_\theta \frac{\partial^2 \bar{\theta}}{\partial z^2} - \frac{1}{\bar{\rho} C_p} \frac{\partial Q^*}{\partial z} - \frac{\partial(\overline{w' \theta'})}{\partial z}. \quad (6)$$

We integrate this equation from the ground to LTM height and averaged it every 5 min. We obtain an approximation for the radiation at LTM height, which reads:

$$\left. \frac{Q^*}{\bar{\rho} C_p} \right|_{z=LTM} = -\nu_\theta \left. \frac{\partial \bar{\theta}}{\partial z} \right|_{z=0m} + \left. \frac{Q^*}{\bar{\rho} C_p} \right|_{z=0m} - \overline{w' \theta'} \Big|_{z=2m}. \quad (7)$$

It is important to note that the tendency of potential temperature vertically integrated from the surface to the LTM height is much smaller than the other terms and for this reason is neglected.

The second term of this equation is computed by using the temperature measured by the IR120 infrared surface temperature sensor and the lowest thermocouple located at 0.015 m and we approximate ν_θ to the ground molecular diffusion value. Moreover, to estimate the heat flux we use the measurements at the lowest SAT, located at 2 m, even though, it is outside the integration domain. During evening transition,

most of $\left. \frac{Q^*}{\bar{\rho} C_p} \right|_{z=0m}$ and $\left. \frac{Q^*}{\bar{\rho} C_p} \right|_{z=LTM}$ corresponds to longwave radiation. Therefore, considering that the main contributor of the upwelling longwave radiation is the ground, we compute the longwave radiation emitted at the ground using the ground temperature (T_g) measured by the IR120 infrared surface temperature sensor as:

$$\left. \frac{Q^*}{\bar{\rho} C_p} \right|_{z=0m} \simeq Lu \Big|_{z=0} = \varepsilon \sigma_b T_g^4, \quad (8)$$

where ε is the emissivity of the ground (0.986) and σ_b is the Stefan–Boltzmann constant.

To discard LTM produced by variations of the ground characteristics during the LTM period, we analyzed the evolution of ground emissivity by using the measurements of longwave radiation at 0.8 m and temperature at 0.015 m. The results do not show any particular modification during the occurrence of LTM. Moreover, a sensitivity study changing the value of the surface emissivity (Gayevsky, 1952; Arya, 2001) has been also performed without qualitatively modifying the results presented below.

Figure 8a shows the temporal evolution of the upwelling longwave radiation measured by the Kipp & Zonen CNR1 net radiometer at 0.8 m. During afternoon transition, we observe a nearly constant decay rate for the upwelling longwave radiation at 0.8 m. Longwave radiation at the ground calculated by using Eq. 8 presents a similar evolution (not shown). However, we cannot correlate these two upwelling longwave radiations to analyze if there is any difference to explain the appearance of the LTM because the IR120 infrared surface temperature sensor and the longwave net radiation sensor have different response times (< 1 s for the IR120 infrared camera and 18 s for the Kipp & Zonen CNR1 net radiometer). Moreover, both sensors were not sampling using the same data logger. Consequently, we focus on analyzing the differences in the decay rate of upwelling longwave radiation at 0.8 m and the longwave radiation at LTM height calculated by using Eq. 7.

Figure 8b shows the temporal evolution of the longwave radiation at the LTM height estimated by using Eq. 7. This figure does not include the longwave radiation at the LTM height for 27 and 30 June 2011 because presented some problems the IR surface temperature sensor measurements during these IOPs. In contrast to Fig. 8a, the longwave radiation decay rate is not constant and increases around 17:30–18:30 UTC, when the LTM appears for some IOPs. This increase in the longwave radiation decay rate can lead to a more rapid local decrease in air temperature and the formation of a LTM.

It is important to note that with the deployed instruments during the campaign, we are not able to study the vertical profile of the air emissivity. We use longwave radiation measured at 0.8 m and the closest measurements of temperature (2 m) to estimate air emissivity and no variation of the air emissivity occurred around the time of the LTM for any of the analyzed days (not shown).

Mukund et al. (2010) reported that LTM–intensity decreases when clouds were present, also suggesting the importance of radiation in the phenomenon. By analyzing the ceilometer measurements obtained during BLLAST (not shown), a completely clear sky is reported for all IOPs evening transition except on 30 June 2011. From the previous section, we know that during this day even though the conditions of turbulence were acceptable to observe LTM and LTM presented similar values to other IOPs, but there was a combination of low intensity and short duration not present in other IOPs. These LTM–characteristics can be also caused by the presence of clouds.

5 Conclusions

The presence of a Lifted Temperature Minimum during the evening transition is studied by means of observations taken during the BLLAST campaign. The campaign site presented ground characteristics suitable for observing LTM measurements with large ground emissivity and thermal inertia. During this period of the day, LTM measurements were observed at different heights, and with different intensity and duration during all IOPs except on 27 June 2011.

With the instrumentation deployed during the campaign we were not able to verify all the previous hypothesis to explain the appearance of a LTM. For instance, the presence of aerosols at lower height were not monitored during the campaign.

Additionally, it would be difficult to analyze, by using observations, the budget between radiation warming and turbulence cooling during the evening transition. While small Kajo–Denkji sonics could be used at 15 cm and 30 cm to measure cooling via sensible heat flux divergence, radiation measurements would be much more difficult at those heights close to the surface, and not possible with commercial pyranometers.

Additionally, it is important to note that the research study focusses on the afternoon transition. To our knowledge, the heat budget (the competition between turbulent fluxes and radiation divergence) at the different levels close to the surface has not been studied during this period of the day. In fact, the currently MATERHORN observational campaign (Jeglum et al., 2013) was partially designed to study the evolution of the heat budget during the afternoon/evening transition.

By studying the wind conditions characterized by a mountain–plain flow, we conclude that the days with a more marked decrease of mean wind speed and wind speed fluctuations (24 June or 1 July 2011) have a more intense LTM. On the other hand, on the days without a reduction of wind speed, such as 27 June 2011, LTM measurements cannot be observed during the evening transition.

Analyzing Ri_g during the evening transition, we observe that the LTM is detected on days with a faster increase of

Ri_g , i.e. a faster decrease of mechanical turbulence. However, due to the fact that $\partial\overline{\theta}_v/\partial z$ is changing sign during the evening transition, no threshold of Ri_g (Oke, 1970) can be defined.

Finally, the longwave–radiative conditions are analyzed. We study the differences in the decay rate of the upwelling longwave radiation at 0.8 m and the longwave radiation at LTM height. Longwave radiation at LTM height decay in two different rates in contrast to the upwelling longwave radiation decay at 0.8 m which is constant in time. This change in the radiative conditions can modify the temporal evolution of the potential temperature creating the LTM.

To conclude, during evening transition it is possible to observe the Lifted Temperature Minimum over a terrain with moderate/large emissivity and thermal inertia. In this study case, really calm conditions were observed during evening transition due to the presence of the Pyrenees Mountains which produces a early evening calm period easily defined through a change in the wind velocity and turbulence. Moreover, a change in the radiative conditions was observed during LTM period which confirms its radiative origin.

Acknowledgements. This project was performed under the Spanish MINECO projects CGL2009–08609, and CGL2012–37416–C04–03. The MODEM radio sounding station and the UHF wind profiler have been supported by CNRS, Université Paul Sabatier and FEDER program (Contract num. #34172–Development of the instrumentation of Observatoire Midi–Pyrénées–PIRENEA–ESPOIR). The 60–m tower equipment has been supported by CNRS, Université Paul Sabatier and European POCTEFA 720 Flux–Pyr program. One EC station was supported by Wageningen University and two EC stations were supported by the University of Bonn and DFG project SCHU2350/21.

The BLLAST field experiment was made possible thanks to the contribution of several institutions and supports: INSU–CNRS (Institut National des Sciences de l’Univers, Centre National de la Recherche Scientifique, LEFE–IDAO program), Météo–France, Observatoire Midi–Pyrénées (University of Toulouse), EUFAR (European Facility for Airborne Research) and COST ES0802 (European Cooperation in the field of Scientific and Technical). The field experiment would not have occurred without the contribution of all participating European and American research groups, which all have contributed in a significant amount. The BLLAST field experiment was hosted by the instrumented site of Centre de Recherches Atmosphériques, Lannemezan, France (Observatoire Midi–Pyrénées, Laboratoire d’Aérodologie). The BLLAST data are managed by SEDOO, from Observatoire Midi–Pyrénées.

Finally, we would like to thank Prof. K. R. Sreenivas from the Jawaharlal Nehru Centre for Advanced Scientific Research and S. Wacker from the Physikalisch–Meteorologisches Observatorium Davos for fruitful discussions about atmospheric radiation.

References

Arya, S. P.: Introduction to Micrometeorology. Academic Press, San Diego, USA. 420 pp. 2001.

- Bhat, G. S.: Near–surface temperature inversion over the Arabian Sea due to natural aerosols. *Geophys. Res. Lett.*, 33, L02802, doi:10.1029/2005GL024157.
- 680 Campbell, G. C.: Measurement of air temperature fluctuations with thermocouples. Atmospheric Sciences Laboratory, White Sands Missile Range, ECOM-5273, 10 pp. 1969. 740
- Campbell, G. S. and Norman, J. (Eds): *An Introduction to Environmental Biophysics*. Springer, 2 ed., 1998.
- 685 De Coster, O. M. Y. and Pietersen, H. P.: BLLAST–uniform processing of Eddy-Covariance data. Internship Report Meteorology and Climatology, Wageningen University and Research Center, The Netherlands, 30 pp., available at http://bllast.sedoo.fr/documents/reports/H-Pietersen_O-de-Coster_BLLAST-surf_flux-uniform-processing.pdf, 2011. 690
- Edwards, J.M.: Radiative Processes in the Stable Boundary Layer: Part I. Radiative Aspects. *Bound.–Lay. Meteorol.*, 131, 105–126, 2009a. 750
- Edwards, J.M.: Radiative processes in the stable boundary layer: Part II. The development of the nocturnal boundary layer. *Bound.–Lay. Meteorol.*, 131, 127–146, 2009b. 695
- Gayevsky, U.L.: Surface temperature of large territories. *Proc. Main Geophys. Obs.*, 26, 291–310, 1952. 755
- Geiger, R.(Eds.): *The Climate Near the Ground*. Harvard University Press, 1957. 700
- Jeglum, M. E., Fernando, H. J. S., Pardyjak, E. R., Zajic, D., De Wekker, S. F. J., Pace, J. C., Di Sabatino, S., Hoch, S. W., Steenburgh, J.Pu, Z., Whiteman, C. D., Massey, J. D., Wang, Y., Leo, L. S., Hocut, C. M., Zhang, H. and Jensen, D.: The Mountain Terrain Atmospheric Modeling and Observations (MATERHORN) Program: Observations and Results. 15th Conference on Mesoscale Processes (August 6–9, 2013), Portland (OR, USA), 2013. 705
- Lake, J. V.: The temperature profile above bare soil on clear nights. *Q. J. Roy. Meteorol. Soc.*, 82, 187–197, 1956. 710
- Lothou, M., Lohou, F., Pino, D., Couvreux, F., Pardyjak, E. R., Reuder, J., Vilà–Guerau de Arellano, Durand, P., Hartogensis, O., Legain, D., Augustin, P., Gioli, B., Faloon, I., Yagüe, C., Alexander, D., Angevine, W., Bargain, E., Barrié, J., Bazile, E., Bezombes, Y., Bezombes, Y., Blay–Carreras, E., van de Boer, A., Boichard, J. L., Bourdon, A., Butet, A., Campistron, B., de Coster, O., Cuxart, J., Dabas, A., Darbieu, C., Deboudt, K., Delbarre, H., Derrien, S., Flament, P., Fourmentin, M., Garai, A., Gibert, F., Graf, A., Groebner, J., Guichard, F., Jiménez M. A., Jonassen, A., von Kroonenbeerg, M., Lenschow, D., Magliulo, V., Martin, S., Martínez, D., Mastrotrillo, L., Moene, A., Molinos, F., Moulin, E., Pietersen, H., Pigué, B., Pique, E., Román-Gascón, C., Rufin–Soler, C., Saïd, F., Sastre–Marugán, M., Seity, Y., Steeneveld, G. J., Toscano, P., Traullé, O., Tzanos, D., Wacker, S., Wildmann, N., and Zaldei, A.: The BLLAST field experiment: Boundary–Layer Late Afternoon and Sunset Turbulence, *Atmos. Chem. Phys.*, 14, 10931–10960, 2014. 725
- Mukund, V., Ponnulakshmi, V. K., Singh, D. K., Subramanian, G., Sreenivas, K. R.: Hyper-cooling in the nocturnal boundary layer: the Ramdas paradox. *Phys. Scripta*, 142, 014041, 2010. 730
- Mukund, V., Singh, D. K., Ponnulakshmi, V. K., Subramanian, G. and Sreenivas, K. R.: Field and laboratory experiments on aerosol–induced cooling in the nocturnal boundary layer. *Q. J. Roy. Meteorol. Soc.*, 140, 151–169, DOI: 10.1002/qj.2113, 2014.
- Nadeau, D. F., Pardyjak, E. R., Higgins, C. W., Huwald, H., and Parlange, M. B.: Flow during the evening transition over steep Alpine slopes. *Q. J. Roy. Meteorol. Soc.*, 139, 607–624, 2013.
- Narasimha, R.: When and why air can be cooler than ground just below: A theory for the Ramdas effect. *J. Indran. Inst. Sci.*, 71, 475–483, 1991.
- Narasimha, R.: The dynamics of the Ramdas layer. *Curr. Sci. India*, 66, 16–23, 1994.
- Narasimha, R., Vasudeva Murthy, A. S.: The energy balance in the Ramdas layer. *Bound.–Lay. Meteorol.*, 76, 307–321, 1995.
- Oke, T. R. : The temperature profile near the ground on calm clear nights. *Q. J. Roy. Meteorol. Soc.*, 96, 14–23, 1970.
- Ponnulakshmi, V. K., V. Mukund, D. K. Singh, K. R. Sreenivas, G. Subramanian: Hypercooling in the Nocturnal Boundary Layer: Broadband Emissivity Schemes. *J. Atmos. Sci.*, 69, 2892–2905, 2012.
- Ramdas, L.A. and Atmanathan, S.: The vertical distribution of air temperature near the ground at night. *Beitr. Geophys.*, 37, 116–117, 1932.
- Ramdas, L.A. and Atmanathan, S.: Über das nächtliche temperaturminimum über nackten boden in Poona. *Meteorol. Rundsch.*, 10, 1–11, 1957.
- Savijärvi, H.: Radiative and turbulent heating rates in the clear-air boundary layer. *Q. J. Roy. Meteorol. Soc.*, 132: 147–161, 2006.
- Savijärvi, H.: High-resolution simulations of the night-time stable boundary layer over snow. *Q. J. Roy. Meteorol. Soc.*, 140: 1121–1128, 2014.
- Skamarock, W., Klemp, J. B., Dudhia, J., Gill, D. O., Barker, D., Duda, M. G., Huang, X.–Y. and Wang W.: A description of the advanced research WRF version 3. Tech. Rep. 870 NCAR/TN475+STR, NCAR, 2008.
- Stull, R. B. (Eds.): *An Introduction to Boundary Layer Meteorology*. Kluwer Academic Publisher, Dordrecht, The Netherlands, 1988.
- Sun, J., Burns, S.P., Delany, A.C., Oncley, S.P., Horst, T.W., Lenschow, D.H.: Heat balance in the nocturnal boundary layer during CASES–99. *J. Appl. Meteorol.*, 42, 1649–1666, 2003.
- Vasudeva Murthy, A. S., Srinivasan, J., and Narasimha, R.: Theory of the lifted temperature minimum on calm clear nights. *Philos. T. R. Soc. A*, 344, 183–206, 1993.
- Vasudeva Murthy, A. S., Narasimha, R., Varghese, S.: An asymptotic analysis of a simple model for the structure and dynamics of the Ramdas layer. *Pure Appl. Geophys.*, 162, 1831–1857, 2005.
- Whiteman, C.D.: *Mountain meteorology: fundamentals and applications*. Oxford University Press, Oxford, England, 2000.
- Zdunkowski, W.: The nocturnal temperature minimum above the ground. *Beitr. Phys. Atmos.*, 39, 247–253, 1966.

IOP	LTM	LTM height T1 (m)	LTM height T2 (m)	LTM intensity T1 (K)	LTM intensity T2 (K)	LTM duration T1 (min)	LTM duration T2 (min)
24 June 2011	YES	0.131	0.07-0.14	0.35	0.7	18:15–18:25	17:50–18:50
25 June 2011	YES	0.131	0.3	—	0.5	—	17:50–18:20
27 June 2011	NO	—	—	—	—	—	—
30 June 2011	YES	0.131	0.07-0.14	0.3	0.5	17:55–18:15	17:55–18:15
1 July 2011	YES	0.131	0.07-0.14	0.35	0.7	17:35–17:55	17:30–18:20
2 July 2011	YES	0.131	0.07-0.14	0.3	0.5	17:35–18:05	17:10–18:10

Table 1. Characteristics of the LTM at T1 and T2 for all the studied IOPs.

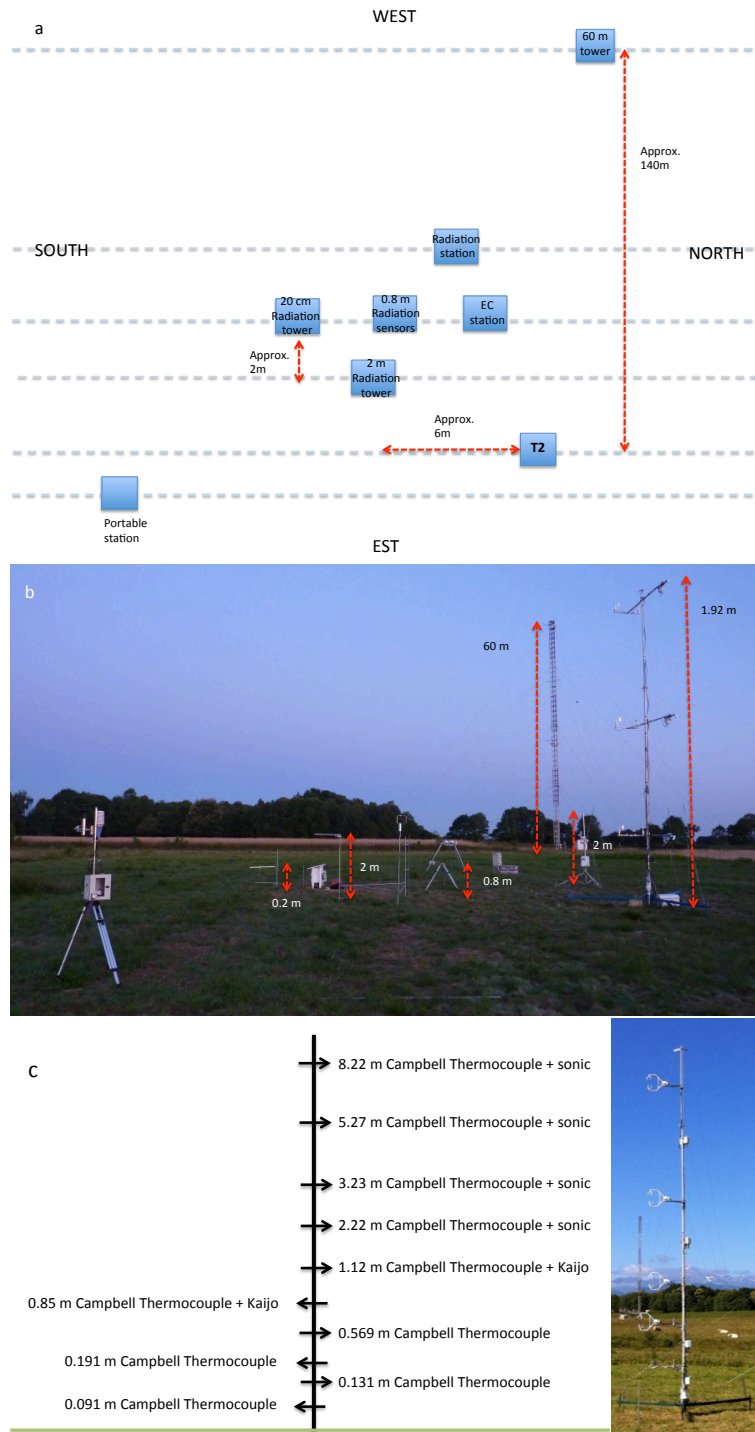


Fig. 1. (a) Schematic horizontal view illustrating the location of the instrumentation around T2 ; (b) photograph (looking west) showing the instruments around T2 and (c) photograph (looking south) showing the instruments around the T1 mast.

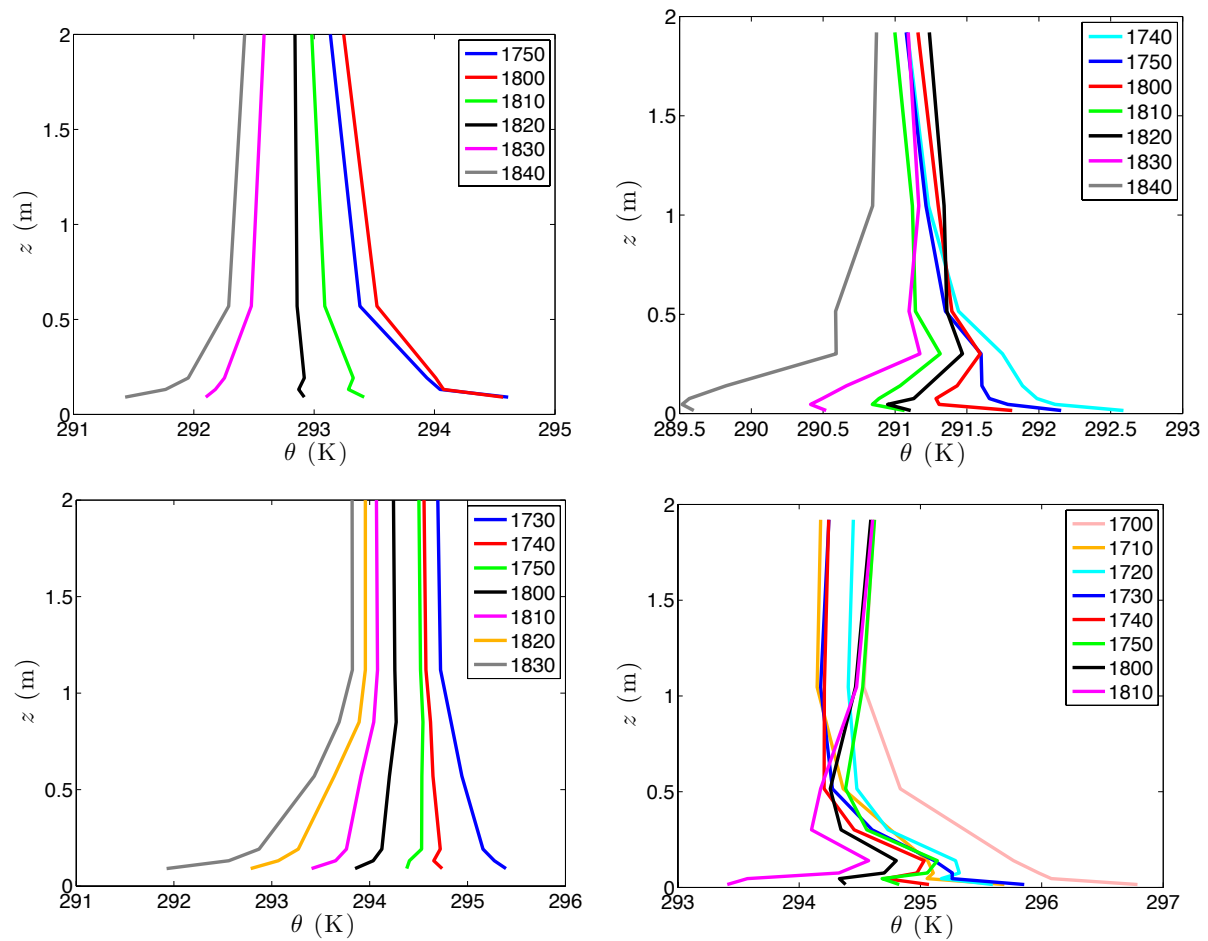


Fig. 2. Temporal evolution of typical vertical potential temperature profiles with an observed LTM on 24 June 2011 (top) and 1 July 2011 (bottom) measured at T1 (left) and T2 (right).

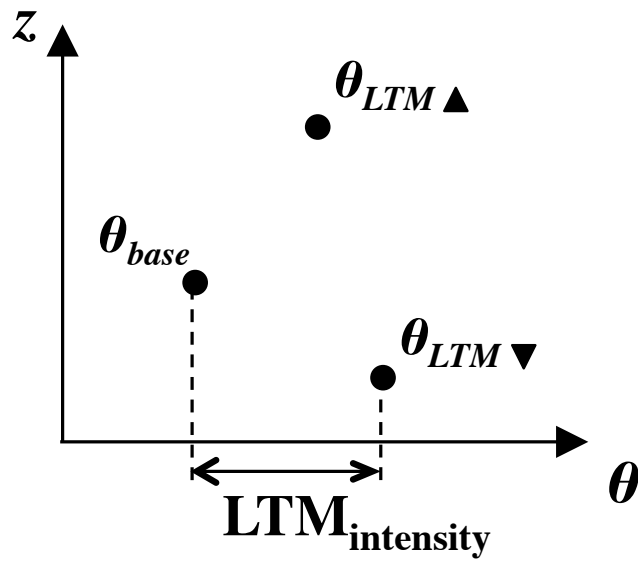


Fig. 3. Illustration of the methodology used to identify LTM and quantify its intensity.

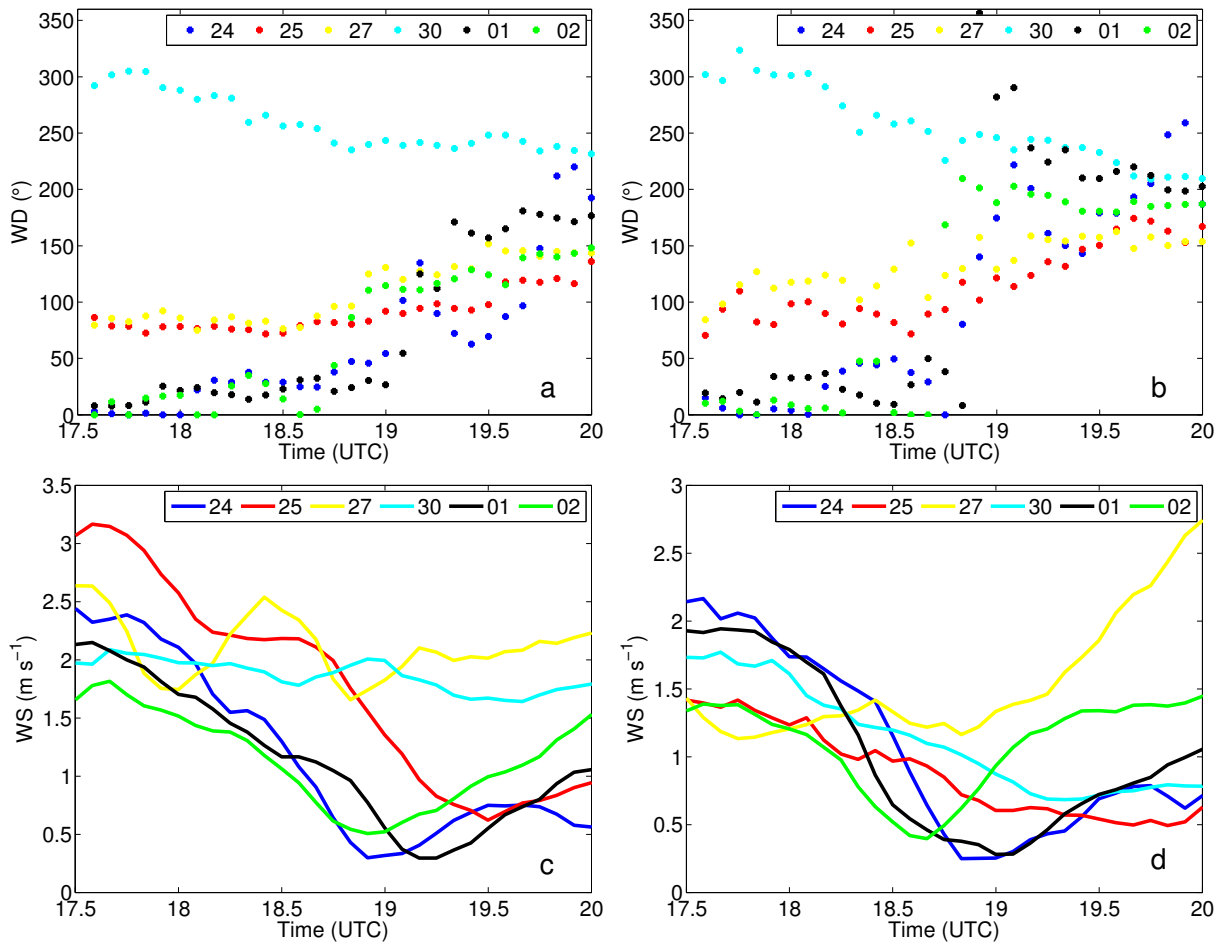


Fig. 4. Temporal evolution, from 17:30 to 20:00 UTC, on all the studied days of the observed 2–m wind direction (top) and speed (bottom) averaged every 5 min at T1 (left) at 2.3 m and T2 (right) at 2 m.

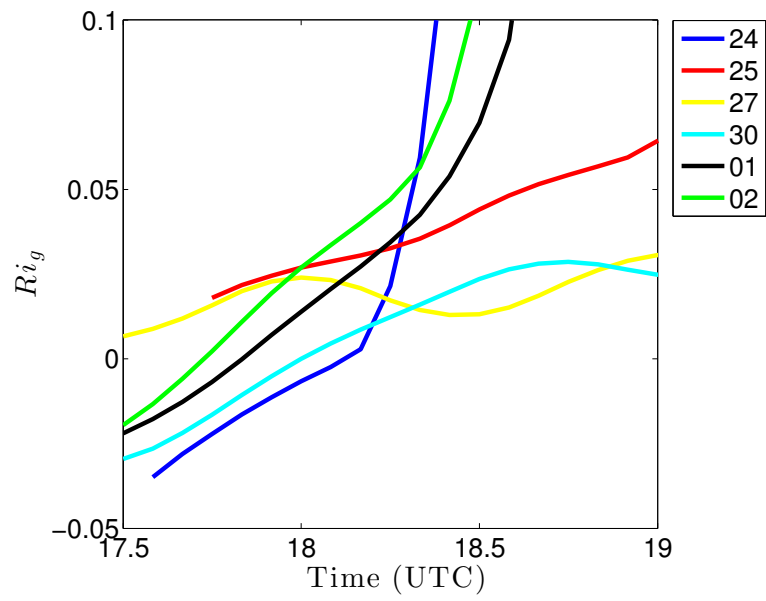


Fig. 5. Temporal evolution of the Richardson number from 17:30 UTC to 19:00 UTC on all the studied days at T1.

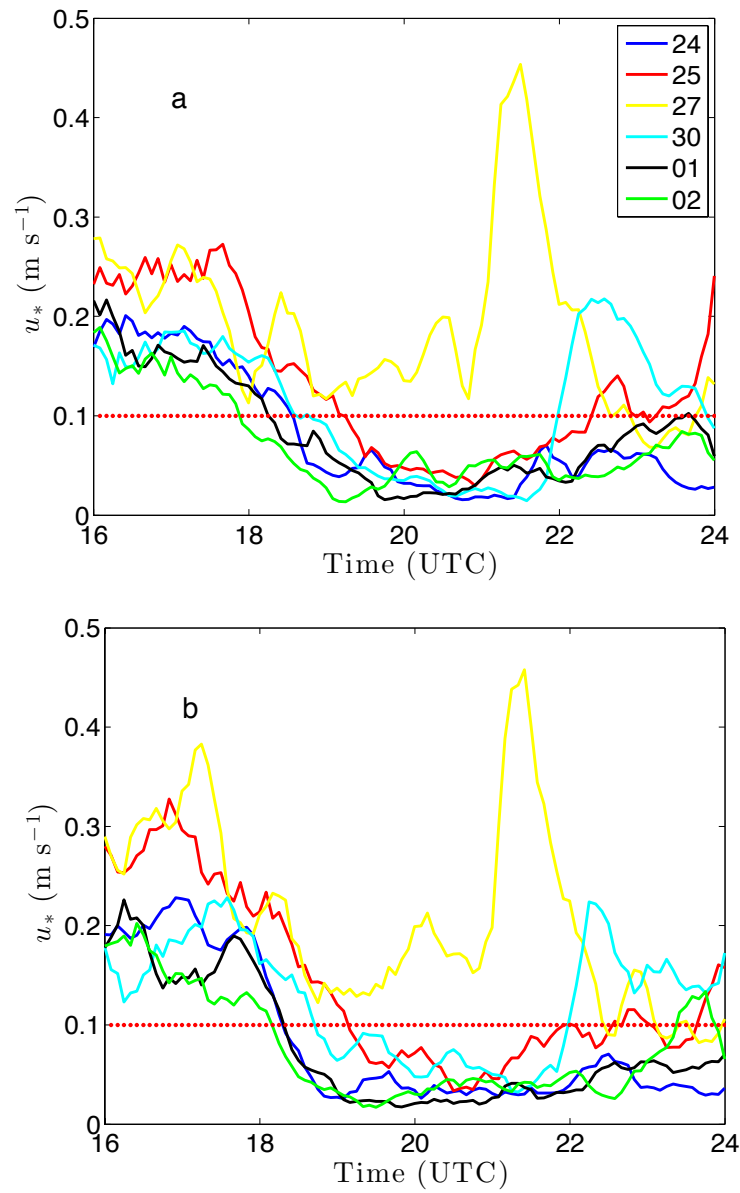


Fig. 6. Temporal evolution of u_* from 16:00 UTC to 24:00 UTC on all the studied days at (a) T1 and (b) T2.

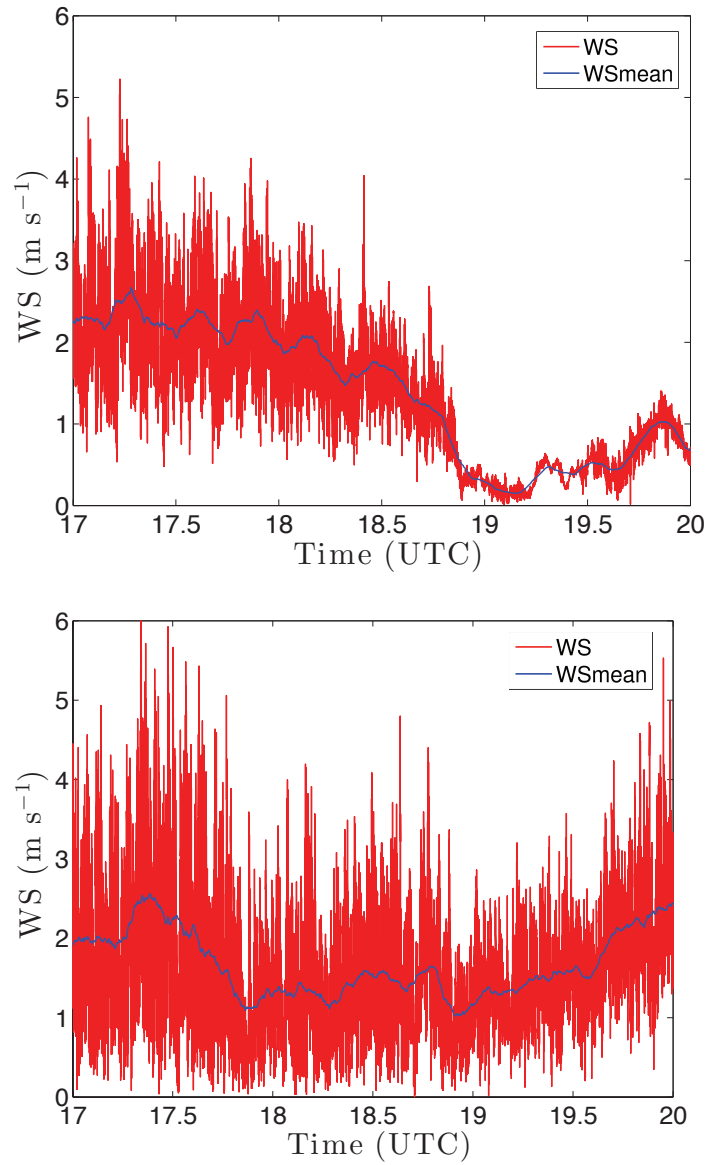


Fig. 7. Temporal evolution of mean wind speed and deviation from mean wind speed on 24 June (top) and 27 June 2011 (bottom).

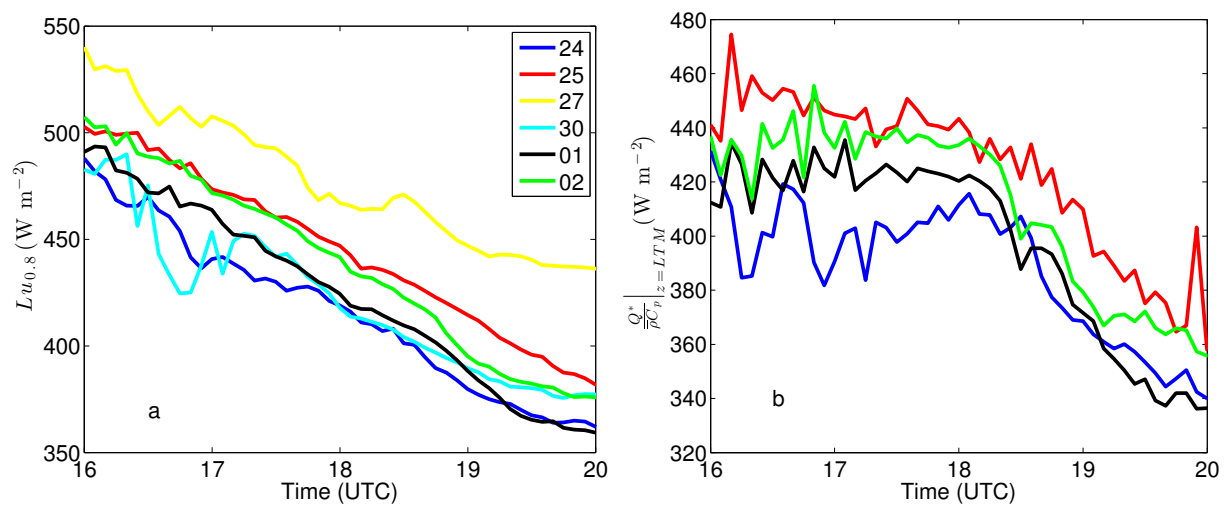


Fig. 8. Temporal evolution of upwards longwave radiation (a) measured at 0.8 m on 24, 25, 27 and 30 June 2011 and 1 and 2 July 2011 and (b) estimated, by using Eq. 7, at LTM height on 24 and 25 June 2011 and 1 and 2 July 2011 using Eq. 7.